UC Irvine

UC Irvine Previously Published Works

Title

Rapid and label-free identification of single leukemia cells from blood in a high-density microfluidic trapping array by fluorescence lifetime imaging microscopy

Permalink

Journal

ISSN

Authors

Lee, Do-Hyun
Li, Xuan
Ma, Ning
et al.

Publication Date

DOI

Copyright Information

Peer reviewed

Check for updates

Rapid and label-free identification of single leukemia cells from blood in a high-density microfluidic trapping array by fluorescence lifetime imaging microscopy†

Do-Hyun Lee, [iD] ‡[a] Xuan Li, [iD] ‡[a] Ning Ma, [iD][ab] Michelle A. Digman [iD] *[ab] and Abraham P. Lee [iD] *[ac]

The rapid screening and isolation of single leukemia cells from blood has become critical for early leukemia detection and tumor heterogeneity interrogation. However, due to the size overlap between leukemia cells and the more abundant white blood cells (WBCs), the isolation and identification of leukemia cells individually from peripheral blood is extremely challenging and often requires immunolabeling or cytogenetic assays. Here we present a rapid and label-free single leukemia cell identification platform that combines: (1) high-throughput size-based separation of hemocytes via a single-cell trapping array, and (2) leukemia cell identification through phasor approach and fluorescence lifetime imaging microscopy (phasor-FLIM), to quantify changes between free/bound nicotinamide adenine dinucleotide (NADH) as an indirect measurement of metabolic alteration in living cells. The microfluidic trapping array designed with 1600 highly-packed addressable single-cell traps can simultaneously filter out red blood cells (RBCs) and trap WBCs/leukemia cells, and is compatible with low-magnification imaging and fast-speed fluorescence screening. The trapped single leukemia cells, e.g., THP-1, Jurkat and K562 cells, are distinguished from WBCs in the phasor-FLIM lifetime map, as they exhibit significant shift towards shorter fluorescence lifetime and a higher ratio of free/bound NADH compared to WBCs, because of their glycolysis-dominant metabolism for rapid proliferation. Based on a multiparametric scheme comparing the eight parameter-spectra of the phasor-FLIM signatures, spiked leukemia cells are quantitatively distinguished from normal WBCs with an area-under-the-curve (AUC) value of 1.00. Different leukemia cell lines are also quantitatively distinguished from each other with AUC values higher than 0.95, demonstrating high sensitivity and specificity for single cell analysis. The presented platform is the first to enable high-density size-based single-cell trapping simultaneously with RBC filtering and rapid label-free individual-leukemia-cell screening through non-invasive metabolic imaging. Compared to conventional biomolecular diagnostics techniques, phasor-FLIM based single-cell screening is label-free, cell-friendly, robust, and has the potential to screen blood in clinical volumes through parallelization.

Introduction

Leukemia, a group of blood cancers that are characterized by the uncontrolled production of abnormal leukocytes from the bone marrow, is the most prevalent pediatric cancer,[1,2] and the sixth most common cause of cancer deaths in the U.S.[3]

Currently, bone marrow aspiration and biopsy are used commonly as standardized procedures for the diagnosis of leukemia and other blood disorders. However, these methods are usually invasive, risky, and difficult for repeat sample acquisitions over an extended time period.[4] Blood-based detection is gentle in comparison and complete blood count (CBC) and peripheral blood smear are relatively quick. Although selective biomarker immunostaining and cytogenetic analysis are able to determine the specific types of leukemia, the procedures are complicated, time-consuming, and expensive.[5–7] There is a critical need in leukemia diagnostics to be able to rapidly and non-invasively isolate single migratory leukemia cells with high sensitivity from unprocessed patient blood samples.

[a] Department of Biomedical Engineering, University of California at Irvine, Irvine, CA, 92697, USA. E-mail: mdigman@uci.edu, aplee@uci.edu; Tel: +949 824 3255, +1 949 824 9691
[b] Laboratory for Fluorescence Dynamics, UC Irvine, CA, USA
[c] Department of Mechanical & Aerospace Engineering, University of California, Irvine, USA
† Electronic supplementary information (ESI) available. See DOI: 10.1039/c7lc01301a
‡ These authors contributed equally to this work.

Microfluidic technology is a powerful tool to process blood samples and isolate circulating tumor cells (CTCs) and leukemia cells in a high-throughput, low cost, and portable manner. In fact, a variety of high-performance microfluidic platforms have been established for isolation and enrichment of CTCs from blood as liquid biopsy, including inertial separation,[8] surface acoustic waves,[9] dielectrophoretic sorting[10] and deterministic chromatography.[11] These techniques are particularly powerful when CTCs have apparent larger diameter than white blood cells (WBCs). However, in the case of separating leukemia cells from blood, the low purity of recovered leukemia cells remains a significant challenge because the size of leukemia cells may exhibit overlap with the size of leukocytes.[12] One approach to improve the selectivity is deformability-based microfluidic discrimination of cancer cells,[13,14] which results in higher-performance cancer cell capture from background cells despite their approximately identical size. In these approaches, however, the strong deformations may damage certain cancer cells due to the high shear stress, and the separation of cells through microstructured constrictions is limited by clogging, which reduces selectivity of cancer cells. Alternatively, cancer cells can be sorted based on epithelial cell surface markers expressed predominantly on cancer cells, such as epithelial cell adhesion molecule (EpCAM). However, the capture efficiency would be heavily dependent on the EpCAM expression level of cancer types and patients.[15,16] Also, recovery of biomarker-conjugated cells from the antibody-coated surface induces leukemia cell damage and requires an additional non-trivial step for culture and enumeration.[17] Jackson and Li et al. separated the peripheral blood to search for circulating leukemic cells[18] and lymphoblasts[19] within the antibody-immobilized microfluidic channel, respectively, but still needed a time-consuming labeling process and have typically yielded low sample purities (<1%), causing challenges in downstream analysis.

To overcome these difficulties of the discrimination and isolation of leukemia cells, the development of label-free technologies to identify and discriminate leukemia cells at a single-cell level has become critical for improving leukemia diagnosis.[20,21] The intrinsic fluorescence of cells generated from endogenous proteins and metabolites is an alternative way to discriminate the cancer cells from normal differentiated cells. The widespread adoption of multiphoton fluorescence imaging and microscopy has followed progressive improvements in label-free and non-invasive detection of cellular metabolism and functional analysis with minimal photo-damage and maximized resolution. For example, the reduced form of nicotinamide adenine dinucleotide (NADH) is one of the main fluorescent metabolic coenzymes involved in oxidative phosphorylation (OXPHOS) and glycolysis, reporting metabolic changes associated with cell carcinogenesis and differentiation. Based on the Warburg effect, tumor cells exhibit increased production of lactate because of an increased rate of glycolysis, in which[22] a large population of free NADH is reproduced instead of a protein-bound form of NADH during electron transferring in OXPHOS. Thus, the ratio of free/bound NADH is lower compared to that in tumor cells. Therefore, label-free, rapid, and noninvasive methods to measure cellular metabolic states and free/bound NADH levels of single leukemia cells are highly desirable in order to separate and detect single leukemia cells from normal blood cells for biomedical applications. Since different fluorophores (e.g., free versus protein-bound forms of NADH) have unique lifetimes independent of their concentration. Given that many cancer cells exhibit increased glycolysis, single cells such as leukemia cells can be discriminated from normal cells based on their fluorescence lifetime signatures with fluorescence lifetime imaging microscopy (FLIM). The phasor algorithm (phasor-FLIM) has been established for fluorescence lifetime data analysis allowing straightforward interpretation of intrinsic fluorescence signals from live tissues directly regarding physiological relevant fluorophores. The advantage of this method is that the time arrival of each photon is collected in every pixel in the image. Although lifetime is independent of the amount of the fluorophore, the absolute concentration of the free and bound NADH cofactor can be determined by using the vector sum of the phasors to correct for the difference in quantum yield states of NADH. This calculation is quantitative, as described by Ma et al.,[23] when a known concentrated standard for the pure free form of NADH is used. Phasor-FLIM is a label-free and fit-free sensitive method to identify metabolic states of cells and can be used to classify stems cells, normal differentiated cells and cancer cells both in vitro and in live tissue.[24]

We report a metabolic-based, label-free leukemia cell identification method that combines (i) passive hydrodynamic control for separation and trapping of single living leukemia cells and normal WBCs parallel in a continuous flow with, (ii) rapid screening of single-leukemia cells from normal WBCs via phasor-FLIM imaging of the single cell intrinsic fluorescence signatures (Fig. 1a).[25] Blood sample is processing via a microfluidic trapping array with 1600 traps that are filled within 3 min. In the phasor-FLIM, each endogenous fluorescence lifetime signature can be distinguished by its distinct location in the phasor plot. We hypothesize that the quantification of free versus bound NADH of isolated single cells presents an opportunity to functionally distinguish metabolically active leukemia cells from normal WBCs in blood. With the combination of a single-cell microfluidic trapping device and the phasor-FLIM, this rapid screening platform enables high-throughput screening of NADH in a large number of cells at single-cell resolution, leading to detection of metabolically active leukemia cells compared to the normal WBCs. To quantify the differences between lifetime distributions of each cell type we produced a multiparametric analysis, as described by Ranjit et al.,[26] to compare between the two spectra comprised of the phasor histogram and distribution calculated from leukemia and normal WBCs for quantitative separation and statistical calculation. To the best of our knowledge, the presented platform is the first to enable high-density single-cell trapping simultaneously with RBC filtering and to achieve rapid
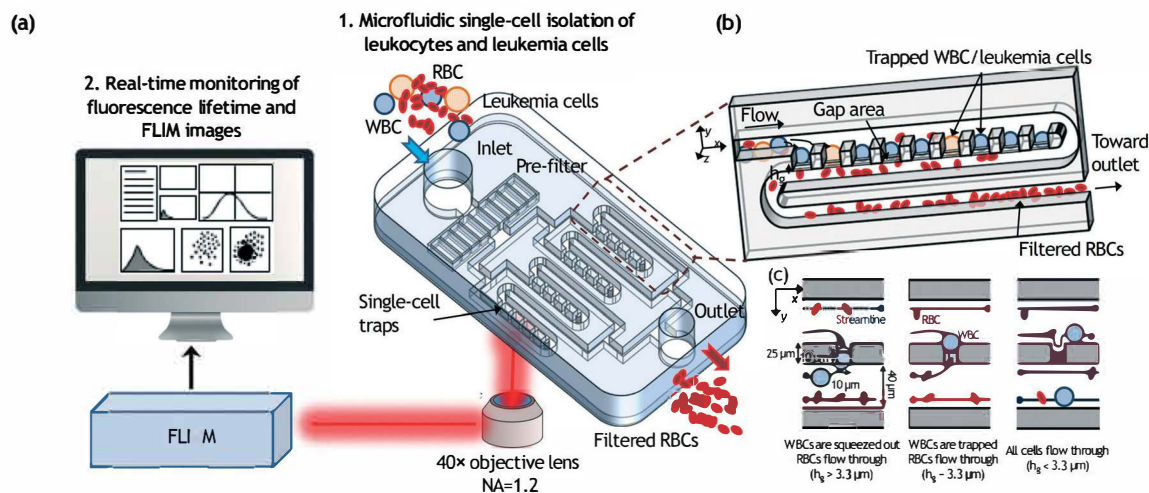
Fig. 1 A microfluidic platform for the label-free isolation and rapid identification of single leukemia cells from blood based on fluorescence life-time imaging microscopy (FLIM). (a) Schematic illustration of the microfluidic platform comprising the hydrodynamic filters and the array of single-cell traps and observation intrinsic single cell signal *via* FLIM. (b) Schematic of the microfluidic single-cell trapping region, in which white blood cells and leukemia cells are trapped in the array individually, while red blood cells are passed through the trap and filtered out at the outlet chamber. (c) Schematic figure represents that different height of gap area affects the capturing single WBCs and leukemia cells and filtering RBCs away.

label-free screening of single leukemia cells through non-invasive metabolic imaging. Compared to conventional biochemical or biomolecular-based diagnostics, the phasor-FLIM based screening opens up new opportunities of using metabolic imaging for *in vitro* diagnostics, which overcomes the limitation of complicated sample processing, high-cost, and cytotoxicity.

Material and methods

Fabrication of the microfluidic device

A microfluidic device was fabricated in PDMS by the soft lithography method and consisted of a pre-filter region and a single-cell trapping region. SU-8 (MicroChem Corp., St. Newton, MA) structures were patterned on a silicon wafer *via* standard multi-step photolithography. Liquid PDMS mixed with a curing agent (ratio of 10:1) was cast on the mold and cured for 3 h in a convection oven at 65 °C for complete cross-linking. Then the PDMS microchannel was irreversibly bonded to a flat glass slide after treatment with oxygen plasma for 60 s. Pillar structures in the inlet channels with a pitch of 25 μm function as pre-filters to prevent the introduction of cancer cell aggregates into the trapping region and separated RBCs are directed to a waste outlet channel. We designed 16 parallel trapping channels to increase the throughput of cell separation and isolation. The height and the width of the main channel were 18 μm and 40 μm, respectively, while the width and length of the traps were both 10 μm.

Cell culture

THP-1 (human acute monocytic leukemia cell line), Jurkat (human acute T cell leukemia cell line), and K562 (human chronic myelogenous leukemia cell line) cells were purchased

from American Type Culture Collection (ATCC), and cultured in RPMI1640 medium (Gibco) supplemented with 10% fetal bovine serum (FBS; Gibco). In particular, for THP-1 cells, 0.05 mM 2-mercaptoethanol (Sigma) was added as a metabolic supplement. Cells were passaged every 2–3 days following standard protocols and cultured in a humidified incubator at 37 °C with 5% CO_2.

Blood samples

De-identified healthy male blood sample was obtained from the Institute for Clinical and Translational Science, Irvine. Vacutainer tubes (BD Bioscience) containing EDTA as an anti-coagulant were used for collection. The blood sample was diluted to 2% hematocrit by adding 1× phosphate buffered saline (PBS) (Life Technologies).

Instrument set-up for imaging

Fluorescence lifetime images of the WBC/leukemia single-cell arrays were acquired utilizing a Zeiss LSM710 microscope coupled with a Ti:sapphire laser system (Mai Tai Spectra-Physics, Newport, CA) and an ISS A320 FastFLIM unit (ISS, Champaign, IL). SimFCS software, developed at the Laboratory of Fluorescence Dynamics (LFD), University of California, Irvine, was used to control the system for FLIM data acquisition. The single-cell array was placed in the 37 °C, 5% CO_2 environment during imaging to ensure cell viability, and was excited *via* two-photon excitation at a wavelength of 740 nm with a laser power of ~5 mW. A 40 × 1.2 NA oil-immersion objective (Carl Zeiss, Oberkochen, Germany) was used, and a dichroic filter (690 nm) separated the fluorescence signal from the laser light. For FLIM image acquisition, fluorescence was detected by a photomultiplier (H7422P-40;

Hamamatsu) using a bandpass filter of 420–500 nm, which covers the emission wavelength of free and protein-bound NADH. Images in the size of 256 × 256 pixels were acquired at the scan speed of 25.21 μs per pixel, and the scanning was continued until 100 counts in the brightest pixel of the images were collected. FLIM calibration of the system was performed by measuring the known lifetime of coumarin 6 (Sigma-Aldrich, St. Louis, MO) dissolved in ethanol which has a single exponential decay of 2.5 ns. Typically, the acquisition time of one selected region of interest in the single cell array, which can include as many as 100 single cells, was less than 1 min.

Theory of phasor-FLIM approach

The acquired FLIM data of the single-cell array was analyzed in a phasor approach using SimFCS software. Briefly, the fluorescence lifetime information from each pixel of the FLIM image was transformed into one point in the phasor plot through Fourier transformation, in which the sine component of the fluorescence intensity decay curve of that pixel was transformed into its s axis coordinate, and the cosine component was transformed to its g axis coordinate in the phasor plot. The detailed theory and mathematical transformation process was explained in the ESI† and previous studies.[25] On the phasor plot, we can use a cursor to highlight a cluster of points that corresponded to the pixels in the FLIM image with a particular lifetime range.

Results

Design and operating principle of the platform

The presented high-density single-cell array consists of a serpentine-shape microfluidic channel with size-selective traps arrayed along each row, by which single WBCs and leukemia cells are captured passively with RBCs filtered out simultaneously due to their smaller size (Fig. 1b). The high-density single-cell array allows the isolation of large numbers of single cells in the detection area for FLIM imaging. At the pre-filter with 25 μm pitch and 18 μm height, the unwanted cell aggregates were successfully blocked, and single leukemia cells, WBCs, and RBCs flowed smoothly into the single-cell trapping region. The cell aggregates would cause the microchannel clogging at the single-cell trapping region and decrease the single-cell occupancy. Under the flow rate of 0.2 mL h^{-1}, only 4.74% of leukemia cell aggregates were flown through the pre-filter. The device operation is based on a single-cell trap capable of passively separating and trapping millions of blood cells simultaneously in less than a minute with a single-cell capturing efficiency of ~80%.[27] Each trapping unit has a smaller height of the trap than the height of the main delivery channel, resulting in a gap area (h_g). The gap area makes the perpendicular flow to deform and migrate RBCs, while WBCs and leukemia cells can be pushed into traps, and the combination of perpendicular deformation and horizontal delivery flow enables the continuous blood cell filtration process. The height of h_g is of critical in

determining the WBC/leukemia capturing efficiency, as larger h_g leads to WBCs/leukemia cells squeezing during RBC filtration, and smaller h_g would prohibit both RBC passing through and WBC/leukemia trapping (Fig. 1c). The presented high-throughput microfluidic trapping array contains 16 identical arrays of highly packed 100 single-cell traps, designed with small dimensions to fit within a microscopic field of view and can be filled within 3 min, enabling the observation and identification of every single leukemia cell flowing through the channel (see Fig. S1†).

Most of the normal WBCs and leukemia cells have a diameter ranging from 8 μm to 20 μm, and there exist significant size overlap based on our measurement of normal human WBCs, and three different types of leukemia cells: THP-1, Jurkat, and K562 (Fig. 2a). But both normal WBCs and leukemia cells are larger than RBCs, which have a disk shape with a diameter of ~6.2–8.2 μm and a thickness at the thickest
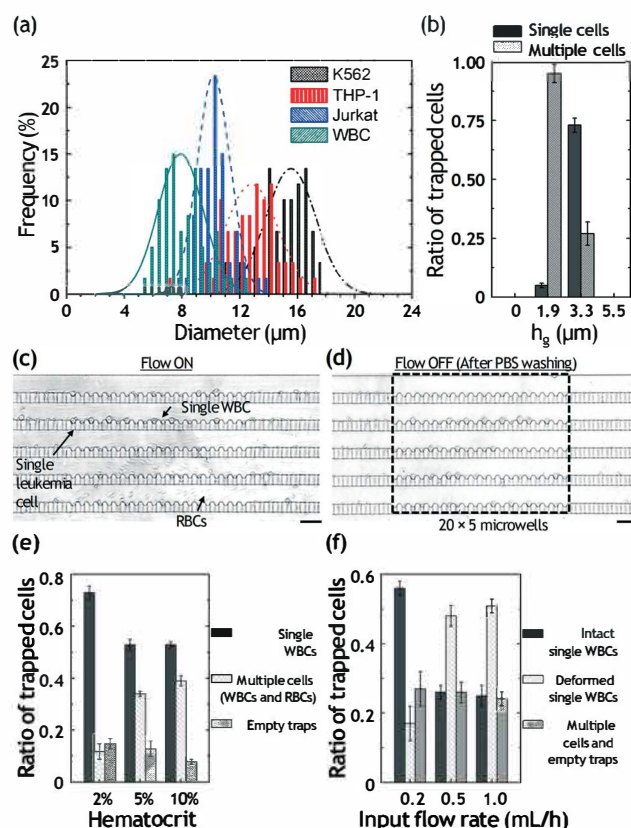

Fig. 2 Cell size characterization and single-cell trapping efficiency optimization. (a) Histogram of the single-cell diameter of WBCs, THP-1, Jurkat, and K562 cells showing the overlap of cell diameter among the WBCs and leukemia cells. (b) The percentage of single-cell occupied traps according to different height of gap area (h_g) of 0, 1.9, 3.3 and 5.5 μm, respectively. (c) Bright-field microscopic image of trapped single WBCs with 2% hematocrit at 0.2 mL h^{-1} input flow rate. (d) RBCs were removed and only WBCs/leukemia cells remained at the microwell array after turning off the sample flow and introducing PBS. (e) Plot showing the percentage of single-cell and multiple-cell occupancy for varying hematocrits. (f) Plot showing the percentage of trapped intact single, deformed single, and multiple WBCs according to the input flow rate. Scale bars: 50 μm.

point of 2–2.5 μm. Therefore, while leukemia cells cannot be separated from WBCs purely by size, RBCs can be successfully filtered out within the microfluidic trapping arrays. We hypothesize that RBCs are not constrained by the gap area constrictions because of their extreme deformability and large surface area compared to WBCs and leukemia cells.[28] We first tested the percentage of single-cell occupied traps according to different h_g of 0, 1.9, 3.3 and 5.5 μm, respectively (Fig. 2b). If h_g is 0, we did not observe any cell trapping within the microwell arrays. We found that the single-cell trapping efficiency was about 73.48% with h_g of 3.3 μm, while no cell was observed at the trap with h_g of 1.9 and 5.5 μm. Especially, when the h_g was much lower than the RBC diameter ($h_g \sim 1.9$ μm), RBCs were stuck at the trap and could not migrate through the gap area, resulting in increased number of multiple-cell trapping. In contrary, when the h_g was much higher than the RBC diameter and similar to the WBC diameter ($h_g \sim 5.5$ μm), all blood cells including WBCs and RBCs were passed through the gap area instead of being trapped in the single microwells. The results demonstrate that the appropriate h_g can filtrate only RBCs and isolate single WBCs as well as cells that have a larger diameter than WBCs such as leukemia cells. Based on these observations, we chose an optimal $h_g \sim 3.3$ μm to operate a device for WBC isolation applications. Fig. 2c shows that the bright-field microscopic image of trapping WBCs and leukemia cells (K562) within the microwell arrays with $h_g = 3.3$ μm. After turning off the sample flow and introducing PBS, all RBCs were removed toward the outlet and only WBCs and leukemia cells remained at the microwell arrays (Fig. 2d). Single-cell isolation of blood under various rheological conditions was explored, demonstrating highly efficient trapping of single leukemia cells and white blood cells in a high-density microwell array (Fig. 2e and f, ESI,† Fig. S2). We chose to introduce 2% hematocrit blood under 0.2 mL h^{-1} for implementing both the throughput and the single-cell isolation performance.

Phasor-FLIM measurement of WBC and leukemia single-cell arrays

Single cells of 4 different populations, WBC (Fig. 3a), THP-1 (Fig. 3b), Jurkat (Fig. 3c), and K562 (Fig. 3d), were trapped in separate microfluidic arrays under the input flow rate of 0.2 mL h^{-1}, respectively, and are excited via two-photon excitation at 740 nm. The transmission images of the single-cell arrays, the magnified images of the selected regions of interest (ROI), and the NADH fluorescence intensity images of the ROI are shown in Fig. 3 from the panel (i) to (iii). We then applied phasor transformation to the acquired FLIM data and plotted the phasor-FLIM pixel plots of the single-cell arrays as shown in Fig. 3 panel (iv). The fluorescence intensity decay at each pixel of the FLIM image was transformed into a single point in the phasor plot (as defined in the Materials and methods section), in which the s and g coordinates for every pixel of the image, Fourier sine versus cosine components of the fluorescence decay curve were plotted on the y and x-axis where the x coordinate spans from 0 to 1 and the
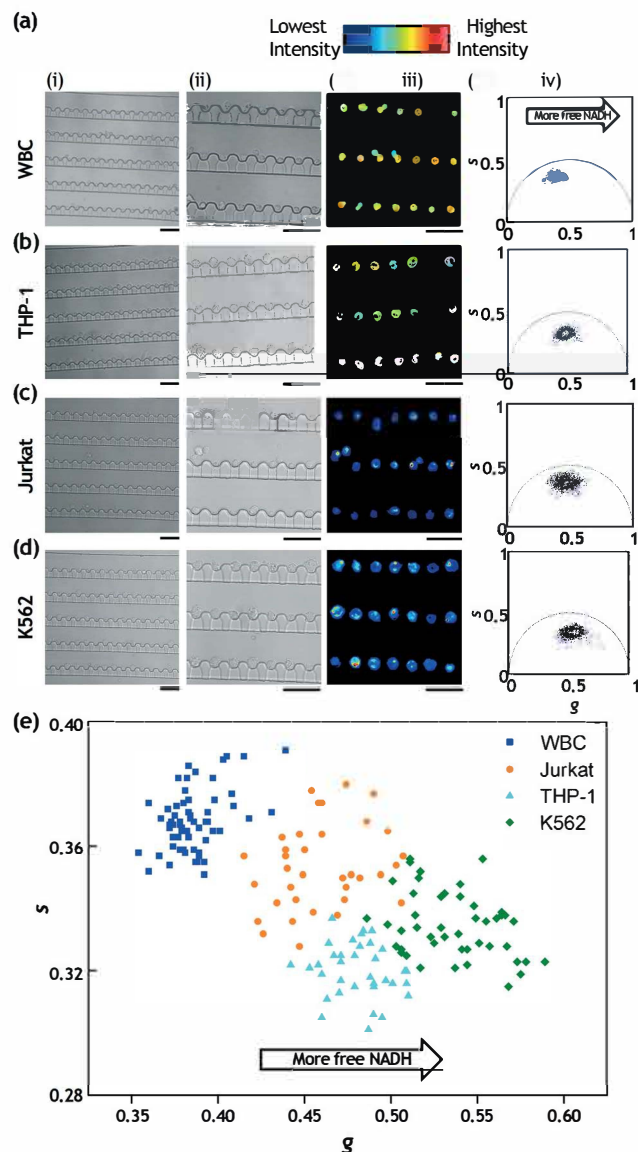

Fig. 3 High-density single-cell trapping and heterogeneous phasor-FLIM signatures of different cell types. (i) Bright-field images, (ii) magnified bright-field images of the selected regions of interest (ROI), (iii) NADH fluorescence emission intensity images, and (iv) corresponding lifetime phasor plots of the single-cell arrays of (a) WBCs, (b) THP-1, (c) Jurkat, and (d) K562 cells. Scale bars: 50 μm. (e) Scatter plot of the average g and s phasor values of trapped single cells based on their NADH fluorescence phasor-FLIM signature. A total number of 65 WBCs (blue), 35 THP-1 cells (cyan), 35 Jurkat cells (orange), and 46 K562 cells (green) are measured and plotted. While the heterogeneity between individual cells among the sample population is observed, all the leukemia cells shifts toward the right compared to WBCs, indicating a higher free-to-bound NADH ratio and a more glycolytic state.

y spans from 0 to 0.5. Based on the pure chemical phasor fingerprints and the linear combination rule,[23,24] signatures of the trapped single WBC and leukemia cells mainly fall between the signatures of the known intrinsic fluorescence biomarkers, free and enzyme-bound forms of NADH being the predominant marker excited at this wavelength, which have a fluorescence lifetime shift from ~0.4 ns at the free stage to

3.2–3.4 ns at the bound stage. To further visualize the difference of the phasor-FLIM signatures between different cell populations and the cellular heterogeneity within the same population, we plotted the average *s* and *g* values of individual cells of WBC (blue square), Jurkat (orange circle), THP-1 (cyan triangle) and K562 (green diamond) in the scatter diagram of Fig. 3e. As shown, the distribution of cell phasors of the WBCs are significantly different from the group of leukemia cells. A comparison of data pairs demonstrated statistically significant differences in cell phasors for each cell types ($p = 3.60 \times 10^{-53}$, Student's *t*-test, *$p < 0.05$). Leukemia cells are shifted toward the lower right direction in the phasor plot compared to WBCs, demonstrating a shorter lifetime, and therefore indicating a higher ratio of free to bound NADH. This can be explained by the Warburg Effect, in which rapid-proliferating tumor-like cells, *i.e.*, leukemia cells, have stronger glycolysis in glucose metabolism to support fast ATP consumption and biosynthesis of macromolecules, therefore have a higher ratio of free/bound NADH; while differentiated cells such as WBCs have stronger OXPHOS and have a higher bound/free NADH ratio. The phasors of the three leukemia cell lines also show inner-population heterogeneity in the scattered plot.

Differentiating different leukemia cell lines *via* multiparametric analysis of phasor-FLIM

While the single-cells' average phasor values of 3 types of leukemia cell lines (THP-1, Jurkat, and K562) were located closely in the scatter plot, they can still be quantitatively differentiated by a multiparametric analysis, or distance analysis[26,29] that splits every cell's phasor points in four equidistance segments based on the height/intensity of the 3D phasor distribution and calculates the average coordinates (*g* and *s*) in each segment (Fig. S3†). A spectrum of 8 parameters specific to the phasor distribution of each cell is created based on the above, and quantitative separation can be applied to the spectra of two different groups, the control (C) and the test (T). The average spectrum of each group and the deviation of each member from the average are calculated: if the spectrum of an unknown cell is equal to the average of C then the separation index (SI) is equal to −10; if it is equal to the average of T then SI = +10; and if the spectrum is at equal distance from C and T then SI = 0.[26,29,30] Cells with a negative or a positive SI value are counted for the control or the test group, respectively, an SI histogram can be plotted based on the number of counts at each SI value. The detailed mathematical explanation of the multiparamic separation is explained in the ESI.† We can also plot the true positive rate against the false positive rate for each separation to get its receiver operating characteristic (ROC) curve and calculate the area-under-the-curve (AUC) value,[31] as a quantitative illustration of the separation's specificity and sensitivity.

As is shown in Fig. 4a, three training sets that separate each 2 of the three leukemia cell lines are established using
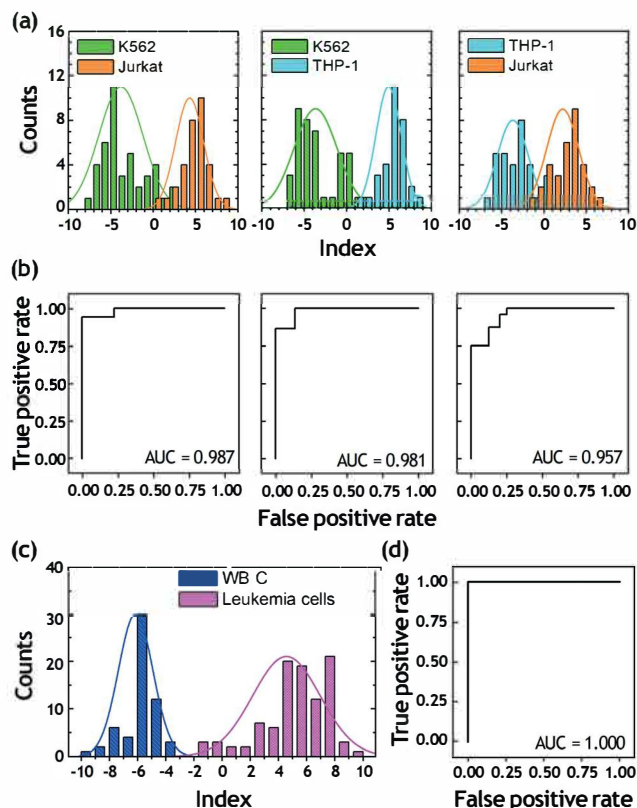

Fig. 4 Separation of WBCs and different types of leukemia cells using multiparametric approach. (a) The separation index (SI) histograms of K562 *versus* Jurkat (right), K562 *versus* THP-1 (middle), and THP-1 *versus* Jurkat (right) demonstrate the efficiency of the multiparametric analysis to distinguish different leukemia cell lines from each other. The SI histogram was plotted based on the number of cell counts against separation index. The SI has a value from −10 to +10. (b) Receiver operating characteristic (ROC) curves constructed by comparing the SI value of two different types of leukemia cells. Values shown are area under the ROC curve (AUC). (c) The SI histogram of WBCs (blue) and the combined leukemia cell population (red) of THP-1, Jurkat, and K562 cells. (d) ROC curves for comparison of WBCs and leukemia cell population.

multiparameter analysis of the cell-line specific phasor distributions, with the SI histograms and ROC curves are plotted, which can be used as a library for further identification of specifice leukemia types in patients' blood. The AUC values of each two comparisons are all higher than 0.950 ($AUC_{THP-1-Jurkat} = 0.957$, $AUC_{K562-THP-1} = 0.981$, and $AUC_{K562-Jurkat} = 0.987$), suggesting a statistically powerful separation between each of the two leukemia cell lines with sufficient sensitivity and specificity (Fig. 4b). Importantly, this classification is performed at a single-cell level rather than as a population metric and across three samples. This multiprapmeteric analysis can also be adopted to broadly separate WBCs from leukemia cells. In Fig. 4c, WBCs are considered as the C group, and all three types of leukemia cells are the T group. While the SI of T group is broadly distributed, indicating the heterogeneity of the leukemia cell population, there is no overlap with the SI distribution of WBCs, and the AUC = 1.000, which means that leukemia cell lines can be clearly

differentiated from WBCs based on the multiparameter scheme, confirming the scatter plot in Fig. 3e (Fig. 4d).

Rapid single leukemia cell screening from leukemia-cell-spiked blood samples *via* phasor-FLIM imaging of the high-density trapping array

After identification of the difference in the phasor-FLIM fingerprints of single WBCs and leukemia cell lines (THP-1, Jurkat, and K562), we conducted the rapid label-free single leukemia cell screening in leukemia-cell-spiked human blood samples. THP-1, Jurkat, and K562 cells were spiked into human blood at a 1 to 5 ratio to WBCs, separately, in order to mimic the blood sample of patients with different types of leukemia, and the diluted whole blood samples (2% hematocrit) were introduced into the high-density single-cell arrays under the flow rate of 0.3 mL h^{-1} (Fig. 5(i)). Then we collected the NADH fluorescence emission of trapped single cells (Fig. 5(ii)) and fluorescence lifetime data at 740 nm, two-photon excitation and plotted the lifetime maps (Fig. 5(iii)) by 1) linking the higher bound/free-NADH-ratio group (red cursor) and the higher free/bound-NADH-ratio group (green cursor) in the phasor distribution plot of all the trapped single cells (Fig. 5d), and 2) color-coding: the color scale from white/cyan to red/pink represents a linear increase of free to protein-bound NADH ratio (Fig. 5e).[32] Different types of the spiked single leukemia cells were clearly distinguished from normal WBCs as highlighted in the white-dashed circles in the lifetime maps (Fig. 5(iii)), as the spiked leukemia cells have more components in the white and blue color, while normal WBCs consist of more red and pink color components. The significant shift toward a higher free/bound NADH ratio and shorter lifetime region of leukemia cells compared to WBCs is because the leukemia cells are in a rapid proliferating stage and utilize more glycolysis to facilitate rapid generation of ATP and biosynthesis of macromolecules, while WBCs use OXPHOS as the major metabolic mechanism to digest glucose more completely but generate ATP slower. Another non-negligible result revealed in the lifetime map is the cell-to-cell heterogeneity among the same population, which represents the unique metabolic pattern of specific cells, and can be further analyzed to separate subpopulations of interest cell type. For example, subgroups of WBCs, *e.g.* neutrophils, eosinophils, basophils, lymphocytes, and monocytes, might be able to be differentiated based on their fluorescence patterns *via* single-cell phasor-FLIM. Apart from color-coding based screening from the lifetime maps, a more quantitative screening of single-leukemia cells can be achieved by loading the phasor-FLIM information to the multiparametric separation training sets that were established in Fig. 4a. As is shown in the SI histogram in Fig. 5f, in which the phasor-FLIM signatures of the single cells (dotted white circle) were compared with WBCs (C group) and the combined population of three leukemia cell lines (T group), and all the circled cells were calculated to have positive SI index values, confirming their identity as leukemia cells. Also, different types of spiked leukemia cells have different SI values within the T group, and the type of a
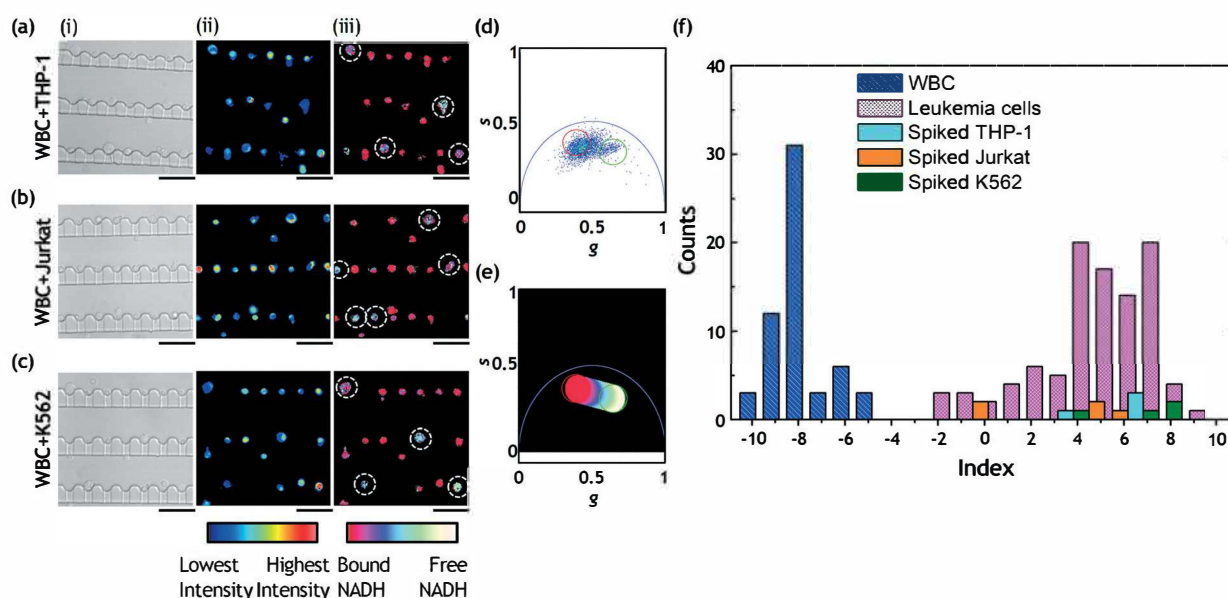

Fig. 5 Screening leukemia cells from normal WBCs in the leukemia cell-spiked blood samples *via* phasor-FLIM imaging of the single-cell trapping array. Panel (i) shows the bright-field images and panel (ii) presents the NADH fluorescence emission intensity images of the THP-1 (a), Jurkat (b), and K562 (c) cells-spiked blood samples, respectively. Scale bars: 50 μm. The phasor distribution of all the trapped single cells is plotted in (d), where the higher bound/free-NADH-ratio group (red cursor) and the higher free/bound-NADH-ratio group (green cursor) are linked and color-coded in (e): the color scale from white/yellow to red/pink represents a linear increase of free to protein-bound NADH ratio. Based on the above, the NADH lifetime maps of the leukemia cell-spiked blood samples are plotted in panel (iii). Leukemia cells demonstrate a significant shift toward a higher free/bound NADH ratio and shorter lifetime indicating a higher glycolytic state. (f) The SI histogram of WBCs (blue), leukemia cells (red), spiked THP-1 (cyan), spiked Jurkat (orange), and spiked K562 (green) cells.

potential known leukemia cell can be further identified by loading its information to the training sets of leukemia cell comparison (Fig. 4b). As the FLIM data collection of each laser scanning area containing 100 single-cell traps takes less than 1 min, the leukemia cell screening of the total 1600 traps could be achieved within 16 min.

Discussion

Here we have shown that our microfluidic single-cell phasor-FLIM platform is capable of trapping both WBCs and leukemia cells while filtering out RBCs and differentiating the similar sized normal leukocytes and leukemia cells by mapping their metabolic fingerprints without any labeling required. The quantitative separation of WBCs and leukemia cells, as well as between different leukemia cell lines, was achieved *via* the established multi-parametric scheme comparing the 8 parameter-spectra of the phasor-FLIM signatures.

One unique innovation in the proposed microfluidic device is that the high-density and high-efficiency cell traps can be utilized as a microfluidic separator of leukocytes and leukemia cells from the diluted blood sample. By filtering out RBCs with smaller sizes and higher deformability, larger leukocytes and leukemia cells are selectively trapped sequentially and individually. The scalable design of high-density single-cell traps speeds up the process of metabolically characterizing a hundred of single cells to screen leukemia in a minute.

Microfluidic single-cell phasor FLIM is particularly relevant to the separation of tumor cells from blood where tumor cells may not be easily discriminated from leukocytes based on size alone. Most microfluidic platforms that separate tumor cells from leukocytes based on size differences lose the majority of smaller sized tumor cells, therefore here we chose to not introduce a size bias in leukemia cell trapping, but to rely on the distinct metabolic difference between normal differentiated cells, *i.e.*, WBCs, and rapidly proliferating tumor cells such as leukemia cells. As is shown in Fig. 3 and 5, there exists a significant difference in the phasor-FLIM signatures between leukemia cells and WBCs, as leukemia cells have shorter fluorescence lifetime and a higher ratio of free to bound NADH, because of their dependence on glycolysis. Also, quantitative separation is achieved (Fig. 4) based on the multiparameter scheme comparing the 8 parameter-spectra of the phasor-FLIM distributions. Both of the above demonstrate that phasor-FLIM based screening is a label-free and robust leukemia cell identification approach, and our platform is the first demonstration to discriminate single leukemia cells from WBCs using phasor-FLIM based on the difference of free/bound NADH ratio. This platform could potentially be useful for discrimination of single activated and non-activated T cells because recent work claims that the Warburg effect is a key process that assist T cell survival and proliferation after activation, as well as produce the effector cytokines.[33] The stimulation of CD8+ T cells boosts rapid production of ROS which has its unique fluorescence lifetime signature in the bottom-left portion of the phasor plot.[34,35] In addition, the activated T cells express a functional phagocyte-type NADPH oxidase, which would shift the FLIM signature towards longer lifetime range.[36] Both of the two aspects lead to a more complex change in FLIM signatures during T cell activation, and should be different from that of tumor cells, which simply shifts towards the shorter lifetime caused by glycolysis. There have been substantial research reporting that leukemic cells are highly glycolytic even though cells reside within the bloodstream which has higher oxygen tension than cells in most normal tissues.[37,38] To expedite leukemia detection and improve personalized therapies, it is crucial to quickly screen the abnormal leukocytes that might allow determination of effective treatment to be made in real time at the bedside. The presented microfluidic isolation platform based on metabolic imaging has advantages over a conventional flow cytometry. Fluorescence-activated cell sorting (FACS) is a representative approach in flow cytometry to categorize heterogeneous samples in a high-throughput manner and is used routinely in clinical diagnosis. But it requires a time and effort consuming process to fluorescently tag cells with expensive antibodies that could potentially lead to irreversible cell damage and change in intrinsic cell properties. In addition, it requires high expense, and need for skilled operating staff. Moreover, the photostability of the fluorophores with time becomes a critical concern along with the broad emission spectra and narrow excitation range of the fluorescent tags. Also, clinical deployment of single leukemia cell monitoring, on the other hand, would require sampling within minutes. Recent FACS machines allows single cell retrieval to negate the issue of requiring subsequent characterization of the sorted populations, but still have a slower throughput than bulk recovery. One of the main challenges in the presented platform is that it can only work with diluted blood. The device can take care of a higher hematocrit level sample and be massively parallelized to move towards higher throughput. We determined that the proposed device could be arrayed with 12 radially arranged channels with successive single-cell traps up to ~6400 traps per unit to avoid the WBC loss integrated into the 3-inch PDMS device that can deal with large volumes of blood samples (Fig. S4†). Based on our calculations, when 2% hematocrit blood is tested at 0.2 mL h^{-1}, ~72 000 single leukemia cells and WBCs can be isolated in 6 min. The high-density single-cell trapping array can be integrated as a multi-step-integration feature with various kinds of microfluidic cell separators. For example, the microfluidic erythrocyte removal modules such as inertial microfluidics,[8] acoustics,[39] and microfilter arrays[11] can be easily combined as an upstream pre-sort sample preparation. This capability is notably crucial when phenotyping of the patient-derived circulating leukemia cells from whole blood is required.

The phasor-FLIM signature heterogeneity within the WBC or leukemia cell population is another non-negligible finding which requires further interpretation. As we know, peripheral WBCs consist of several subpopulations such as lymphocytes,

monocytes, neutrophils, eosinophils, and basophils. Phenotypic and functional analysis of single peripheral WBCs present valuable clinical information based on their numbers, compositions, and functional responses, for example, (i) the production of interferon gamma (IFN-γ) by T-cells which correlates with the immune response against tuberculosis infection, (ii) the increased neutrophil count caused by bacterial infections often cause an increased neutrophil count, while the increased number of lymphocytes due to the viral infections and auto-immune disorders, and (iii) the peripheral blood lymphoblast percentage is an important index for diagnosis and prognosis of acute lymphoblastic leukemia (ALL). Thus the differential counting of WBCs from smaller quantities of blood is crucial for point-of-care diagnosis. Label-free isolation and non-invasive differential discrimination of single leukocytes *via* phasor-FLIM[40] will facilitate *in vitro* analysis of immune responses of single WBCs as an alternative of conventional WBC counting and phenotyping.

The existence of a highly tumorigenic subpopulation of leukemia cells, especially leukemic stem cells (LSCs) in heterogeneous tumor mass plays a role in tumor development, metastasis and construction of the entire spectrum of bulk tumor cells. The current platform based single-cell FLIM identification would be applicable to screen single LSCs according to differential drug responses in the entire tumor population and would enable exploration of tumor heterogeneity and differential response to drugs. After the phenotyping, the single cells of interest can be cultured within the microfluidic device, further analyzed *in situ* and retrieved upon adapting various techniques such as optical DEP,[41] pipetting,[42] and laser-based manipulation.[43] Cellular information from isolated single living leukemia cells can be extracted and/or inserted *via* selective intracellular probing using a dielectrophoretic nanotweezer (DENT)[44] after the phasor-FLIM analysis. This can enable functional characterization of the protein encoded by the introduced DNA to help elucidate how leukemia cells function.

Conclusions

In summary, we have developed a novel leukemia cell screening platform that combines microfluidic single-cell trapping and label-free leukemia cell identification *via* phasor-FLIM imaging. The microfluidic array has 1600 highly-packed single-cell traps which can be filled within 3 min, with the gap height (h_g) of 3.3 μm at each trapping unit to simultaneously filter out RBCs and capture WBCs and leukemia cells from 2% hematocrit blood. By imaging the single-cell array at 740 nm two-photon excitation and getting its fluorescence emission, the trapped single leukemia cells, *e.g.* THP-1, Jurkat and K562 cells, were successfully distinguished from WBCs in the phasor-FLIM pixel map based on their significant shift towards shorter fluorescence lifetime. The higher ratio of free/bound NADH from leukemia cells compared to WBCs was because of their high glycolysis for rapid proliferation. Quantitative separation between WBCs and leukemia cells (AUC =

1.00) as well as between different leukemia cell lines (AUC > 0.95) was achieved with good sensitivity and specificity *via* the established multiparametric scheme comparing the 8 parameter-spectra of the phasor-FLIM signatures. Intrapopulation heterogeneity were also observed through the cell–cell variation of phasor-FLIM signatures. Our platform is the first to enable high-density single-cell trapping simultaneously with RBC filtering and to achieve rapid label-free individual-leukemia-cell screening through non-invasive metabolic imaging. Phasor-FLIM based screening on a high-density trapping array is label-free, cell-safe, quantitative, and it has the potential to screen blood in clinical volumes through parallelization and is expected to be widely used regarding early leukemia/tumor detection, tumor heterogeneity identification, and personalized therapy.

Conflicts of interest

There are no conflicts to declare.

Acknowledgements

References

1 M. Cristofanilli, G. T. Budd, M. J. Ellis, A. Stopeck, J. Matera, M. C. Miller, J. M. Reuben, G. V. Doyle, W. J. Allard and L. W. Terstappen, *N. Engl. J. Med.*, 2004, 351, 781–791.

2 J. F. Bishop, J. P. Matthews, G. A. Young, J. Szer, A. Gillett, D. Joshua, K. Bradstock, A. Enno, M. M. Wolf and R. Fox, *Blood*, 1996, 87, 1710–1717.

3 R. L. Siegel, K. D. Miller and A. Jemal, *Ca-Cancer J. Clin.*, 2016, 66, 7–30.

4 S. P. Sah, E. Matutes, A. C. Wotherspoon, R. Morilla and D. Catovsky, *J. Clin. Pathol.*, 2003, 56, 129–132.

5 M. Faham, J. Zheng, M. Moorhead, V. E. Carlton, P. Stow, E. Coustan-Smith, C. H. Pui and D. Campana, *Blood*, 2012, 120, 5173–5180.

6 B. Falini, M. P. Martelli, N. Bolli, R. Bonasso, E. Ghia, M. T. Pallotta, D. Diverio, I. Nicoletti, R. Pacini, A. Tabarrini, B. V. Galletti, R. Mannucci, G. Roti, R. Rosati, G. Specchia, A. Liso, E. Tiacci, M. Alcalay, L. Luzi, S. Volorio, L. Bernard, A. Guarini, S. Amadori, F. Mandelli, F. Pane, F. Lo-Coco, G. Saglio, P. G. Pelicci, M. F. Martelli and C. Mecucci, *Blood*, 2006, 108, 1999–2005.

7 G. S. Nowakowski, J. D. Hoyer, T. D. Shanafelt, C. S. Zent, T. G. Call, N. D. Bone, B. Laplant, G. W. Dewald, R. C. Tschumper, D. F. Jelinek, T. E. Witzig and N. E. Kay, *J. Clin. Oncol.*, 2009, 27, 1844–1849.

8 M. E. Warkiani, B. L. Khoo, L. Wu, A. K. P. Tay, A. A. S. Bhagat, J. Han and C. T. Lim, *Nat. Protoc.*, 2016, **11**, 134–148.

9 P. Li, Z. Mao, Z. Peng, L. Zhou, Y. Chen, P.-H. Huang, C. I. Truica, J. J. Drabick, W. S. El-Deiry and M. Dao, *Proc. Natl. Acad. Sci. U. S. A.*, 2015, **112**, 4970–4975.

10 P. R. Gascoyne, J. Noshari, T. J. Anderson and F. F. Becker, *Electrophoresis*, 2009, **30**, 1388–1398.

11 N. M. Karabacak, P. S. Spuhler, F. Fachin, E. J. Lim, V. Pai, E. Ozkumur, J. M. Martel, N. Kojic, K. Smith and P.-I. Chen, *Nat. Protoc.*, 2014, **9**, 694–710.

12 F. A. Coumans, G. van Dalum, M. Beck and L. W. Terstappen, *PLoS One*, 2013, **8**, e61770.

13 E. S. Park, C. Jin, Q. Guo, R. R. Ang, S. P. Duffy, K. Matthews, A. Azad, H. Abdi, T. Todenhöfer and J. Bazov, *Small*, 2016, **12**, 1909–1919.

14 M. J. Rosenbluth, W. A. Lam and D. A. Fletcher, *Lab Chip*, 2008, **8**, 1062–1070.

15 M.-H. Park, E. Reátegui, W. Li, S. N. Tessier, K. H. Wong, A. E. Jensen, V. Thapar, D. Ting, M. Toner and S. L. Stott, *J. Am. Chem. Soc.*, 2017, **139**, 2741–2749.

16 S. L. Stott, C.-H. Hsu, D. I. Tsukrov, M. Yu, D. T. Miyamoto, B. A. Waltman, S. M. Rothenberg, A. M. Shah, M. E. Smas and G. K. Korir, *Proc. Natl. Acad. Sci. U. S. A.*, 2010, **107**, 18392–18397.

17 W. Sheng, T. Chen, R. Kamath, X. Xiong, W. Tan and Z. H. Fan, *Anal. Chem.*, 2012, **84**, 4199–4206.

18 J. M. Jackson, J. B. Taylor, M. A. Witek, S. A. Hunsucker, J. P. Waugh, Y. Fedoriw, T. C. Shea, S. A. Soper and P. M. Armistead, *Analyst*, 2016, **141**, 640–651.

19 W. Li, Y. Zhang, C. P. Reynolds and D. Pappas, *Anal. Chem.*, 2017, **89**, 7340–7347.

20 M. Hassoun, J. Rüger, T. Kirchberger-Tolstik, I. W. Schie, T. Henkel, K. Weber, D. Cialla-May, C. Krafft and J. Popp, *Anal. Bioanal. Chem.*, 2018, **410**, 999–1006.

21 A. Pallaoro, M. R. Hoonejani, G. B. Braun, C. D. Meinhart and M. Moskovits, *ACS Nano*, 2015, **9**, 4328–4336.

22 A. Chiarugi, C. Dölle, R. Felici and M. Ziegler, *Nat. Rev. Cancer*, 2012, **12**, 741–752.

23 N. Ma, M. A. Digman, L. Malacrida and E. Gratton, *Biomed. Opt. Express*, 2016, **7**, 2441–2452.

24 C. Stringari, A. Cinquin, O. Cinquin, M. A. Digman, P. J. Donovan and E. Gratton, *Proc. Natl. Acad. Sci. U. S. A.*, 2011, **108**, 13582–13587.

25 M. A. Digman, V. R. Caiolfa, M. Zamai and E. Gratton, *Biophys. J.*, 2008, **94**, L14–L16.

26 S. Ranjit, A. Dvornikov, M. Levi, S. Furgeson and E. Gratton, *Biomed. Opt. Express*, 2016, **7**, 3519–3530.

27 K. Chung, Y. Kim, J. S. Kanodia, E. Gong, S. Y. Shvartsman and H. Lu, *Nat. Methods*, 2011, **8**, 171–176.

28 H. Noguchi and G. Gompper, *Proc. Natl. Acad. Sci. U. S. A.*, 2005, **102**, 14159–14164.

29 S. Ranjit, A. Dvornikov, E. Dobrinskikh, X. Wang, Y. Luo, M. Levi and E. Gratton, *Biomed. Opt. Express*, 2017, **8**, 3143–3154.

30 S. Kukreti, A. Cerussi, B. Tromberg and E. Gratton, *J. Biomed. Opt.*, 2007, **12**, 020509.

31 D. M. Powers, *J. Mach. Learn. Tech.*, 2011, **2**, 37–63.

32 S. Sameni, A. Syed, J. L. Marsh and M. A. Digman, *Sci. Rep.*, 2016, **6**, 34755.

33 M. G. Vander Heiden, L. C. Cantley and C. B. Thompson, *Science*, 2009, **324**, 1029–1033.

34 A. Bai, A. Moss, S. Rothweiler, M. S. Longhi, Y. Wu, W. G. Junger and S. C. Robson, *Nat. Commun.*, 2015, **6**, 8819.

35 R. Datta, C. Heylman, S. C. George and E. Gratton, *Biomed. Opt. Express*, 2016, **7**, 1690–1701.

36 S. H. Jackson, S. Devadas, J. Kwon, L. A. Pinto and M. S. Williams, *Nat. Immunol.*, 2004, **5**, 818–827.

37 S. Gottschalk, N. Anderson, C. Hainz, S. G. Eckhardt and N. J. Serkova, *Clin. Cancer Res.*, 2004, **10**, 6661–6668.

38 E. Hulleman, K. M. Kazemier, A. Holleman, D. J. Vander Weele, C. M. Rudin, M. J. Broekhuis, W. E. Evans, R. Pieters and M. L. Den Boer, *Blood*, 2009, **113**, 2014–2021.

39 Y. Chen, M. Wu, L. Ren, J. Liu, P. H. Whitley, L. Wang and T. J. Huang, *Lab Chip*, 2016, **16**, 3466–3472.

40 C. Li, R. K. Pastila, C. Pitsillides, J. M. Runnels, M. Puoris'haag, D. Côté and C. P. Lin, *Opt. Express*, 2010, **18**, 988–999.

41 H. Hwang, D.-H. Lee, W. Choi and J.-K. Park, *Biomicrofluidics*, 2009, **3**, 014103.

42 B. Dura, M. M. Servos, R. M. Barry, H. L. Ploegh, S. K. Dougan and J. Voldman, *Proc. Natl. Acad. Sci. U. S. A.*, 2016, **113**, E3599–E3608.

43 G. To'a Salazar, Y. Wang, G. Young, M. Bachman, C. E. Sims, G. Li and N. L. Allbritton, *Anal. Chem.*, 2007, **79**, 682–687.

44 X. Li, Y. Tao, D.-H. Lee, H. K. Wickramasinghe and A. P. Lee, *Lab Chip*, 2017, **17**, 1635–1644.